Am J Physiol Endocrinol Metab 307: E161–E175, 2014.
First published May 20, 2014; doi:10.1152/ajpendo.00446.2013.

Etiology of the membrane potential of rat white fat adipocytes

Donna C. Bentley, Pawitra Pulbutr, Sue Chan, and Paul A. Smith

School of Life Sciences, University of Nottingham, Nottingham, United Kingdom

Submitted 15 August 2013; accepted in final form 20 May 2014

Bentley DC, Pulbutr P, Chan S, Smith PA. Etiology of the membrane potential of rat white fat adipocytes. *Am J Physiol Endocrinol Metab* 307: E161–E175, 2014. First published May 20, 2014; doi:10.1152/ajpendo.00446.2013.—The plasma membrane potential (*V*m) is key to many physiological processes; however, its ionic etiology in white fat adipocytes is poorly characterized. To address this question, we employed the perforated patch current clamp and cell-attached patch clamp methods in isolated primary white fat adipocytes and their cellular model 3T3-L1. The resting *V*m of primary and 3T3-L1 adipocytes were -32.1 ± 1.2 mV ($n = 95$) and -28.8 ± 1.2 mV ($n = 87$), respectively. *V*m was independent of cell size and fat content. Elevation of extracellular K^+ to 50 mM by equimolar substitution of bath Na^+ did not affect *V*m, whereas substitution of bath Na^+ with the membrane-impermeant cation *N*-methyl-D-glucamine$^+$-hyperpolarized *V*m by 16 mV, data indicative of a nonselective cation permeability. Substitution of 133 mM extracellular Cl^- with gluconate-depolarized *V*m by 25 mV, whereas Cl^- substitution with I^- caused a -9 mV hyperpolarization. Isoprenaline (10 μM), but not insulin (100 nM), significantly depolarized *V*m. Single-channel ion activity was voltage independent; currents were indicative for Cl^- with an inward slope conductance of 16 ± 1.3 pS ($n = 11$) and a reversal potential close to the Cl^- equilibrium potential, -29 ± 1.6 mV. Although the reduction of extracellular Cl^- elevated the intracellular Ca^{2+} of adipocytes, this was not as large as that produced by elevation of extracellular K^+. In conclusion, the *V*m of white fat adipocytes is well described by the Goldman-Hodgkin-Katz equation with a predominant permeability to Cl^-, where its biophysical and single-channel properties suggest a volume-sensitive anion channel identity. Consequently, changes in serum Cl^- homeostasis or the adipocyte's permeability to this anion via drugs will affect its *V*m, intracellular Ca^{2+}, and ultimately its function and its role in metabolic control.

adipocyte; white fat; 3T3-L1 cells; chloride; membrane potential

THE PLASMA MEMBRANE POTENTIAL (*V*m) is a fundamental biological property for the survival and function of virtually every eukarocytic cell. In excitable tissues of animalia, such as the heart, muscles, and nerves, excursions in *V*m in the form of action potentials represent the fastest known biological means of intraorganism communication. The action potential often acts to mediate intracellular signaling; for example, an associated influx of extracellular Ca^{2+} controls functions as diverse as contraction to secretion. In nonexcitable tissues, subtle changes in *V*m are involved in the control of the transmembrane and transcellular fluxes of many solutes. Moreover, the membrane potential per se also has an important role to play in basic cell homoeostasis: the regulation of intracellular ionic composition and the maintenance of osmotic equilibrium. A thorough understanding of the etiology of *V*m permits us to accurately control it experimentally, a process that allows us to investigate associated physiological and pathological sequelae.

Address for reprint requests and other correspondence: P. A. Smith, School of Life Sciences, Univ. of Nottingham, Nottingham, UK (e-mail: Paul.a.smith@nottingham.ac.uk).

*V*irtually all types of mammalian cell possess a negative membrane potential, ranging from -8 mV in red blood cells (26) to in excess of -90 mV in skeletal muscle (23). The resting membrane potential is a thermodynamic steady-state situation where there is no net flux of electrical charge across the plasma membrane. The *V*m arises through a complex biological calculation performed at the level of the plasma membrane that involves the electrochemical ion gradients, transmembrane ion permeabilities, ion exchange, and electrogenic pump processes (22). For most cell types, the major ion species involved in control of the resting membrane potential are K^+, Na^+, Ca^{2+}, and Cl^-, with the selective ionic permeabilities and related molecular components, such as ion pumps and exchanges, of the plasma membrane reflecting this.

White fat cells are no exception to the possession of a *V*m, although white fat adipocytes are reported to possess a resting membrane potential of between -17 and -69 mV (Table 1); although its exact ionic etiology is still undefined due to various shortfalls in the previous methodologies employed for its study (6, 7). Consequently, the assumption that the adipocyte *V*m arises primarily due to a predominant plasma membrane permeability to K^+ (6, 7) has led workers to use protocols where it is assumed that manipulation of the extracellular concentration of K^+ will modulate adipocyte *V*m and affect membrane transport processes, in particular the transmembrane flux of Ca^{2+} (15, 17, 29, 36, 50). Although such manipulations may indeed increase intracellular Ca^{2+} (29), this effect may not necessarily arise via depolarization of the plasma membrane and voltage-gated Ca^{2+} influx; an increase in intracellular Ca^{2+} can also arise through osmotic shrinkage, reverse-mode Na^+-Ca^{2+} exchange, or necrosis. The possible inappropriate use of high extracellular K^+ to elevate intracellular Ca^{2+} is especially pertinent when interpreting previous studies that have employed this methodology to investigate the role of intracellular Ca^{2+} signaling in the physiological functions of white fat adipocytes: insulin-stimulated glucose uptake and lipogenesis (29), β-adrenoceptor-mediated lipolysis (17, 50), and secretion of various adipokines such as leptin, adiponectin, and resistin (51), especially pertinent events given the clinical importance of understanding the function and physiology of white fat adipocytes in diabesity.

The aim of this study was to characterize the ionic mechanism of the *V*m in unequivocally identified white fat adipocytes. In doing so, we sought to provide values of *V*m for future reference. Furthermore, these data, when combined with published radioisotope ion flux data, allow quantification of the major ionic permeabilities of the adipocyte and provide a clearer picture of ion transport processes across the plasma membrane of this cell type. Moreover, changes that may occur on the *V*m of these cells produced by the two main regulators of adipocyte function, insulin and epinephrine, can be identified and characterized. Finally, we aimed to determine robust

Table 1. *Measurement of membrane potential in cells of rat epididymal fat pads*

*V*m (mV)	Technique	Preparation	Reference
−29	$^{36}Cl^-$ distribution	Isolated cells	33
−17 to −69	Microelectrode	Explant	5
−27 to −29	Microelectrode	Explant	7
−46	Microelectrode	Explant	44
−34	Microelectrode	Explant	39
−30	Microelectrode	Isolated cells	28

For these studies, isolated cells, cells in intact segments, or explants of epididymal fat pads were used as indicated.

protocols that are appropriate for experimental modulation of adipocyte *V*m and intracellular Ca^{2+}.

MATERIALS AND METHODS

For this study, we used primary adipocytes isolated from epididymal fat pads and 3T3-L1 adipocytes, a well-established differentiated fibroblastic model of white fat (20, 21).

Preparation of primary white fat adipocytes. Primary adipocytes were isolated from the epididymal fat pads (41) of both Wistar and Sprague-Dawley strains of rat. Male rats, 250–340 g, fed ad libitum (Charles River Laboratory, Kent, UK) were killed by cervical dislocation after stunning in accordance with UK Home Office guidelines. The epididymal fat pads were excised, the epididymis and major blood vessels expurgated, and the fat pads minced with scissors. Adipocytes were liberated from the mince by 6- to 8-min collagenase digestion: 1 mg/ml Type II collagenase (Sigma cat. no. C6885) in Hank's solution (0.5% BSA wt/vol) at 37°C with mild agitation. The digest was filtered through a 250 μM nylon mesh (Normesh, Oldham, UK), followed by 50 ml of Hank's solution, and the filtrate was collected in an inverted 50-ml syringe. Adipocytes separated from the buffer by flotation to form a white layer on top of the filtrate, whereas cell debris and other cell types precipitated out. The infranatant and debris were removed by drainage, and the separation process was repeated twice more by further buffer additions and drainage. After the final drain, the adipocytes were resuspended in Hank's solution and kept at room temperature (21–22°C) prior to use. For experiments, adipocytes were plated onto glass coverslips coated with poly-D-lysine (100 μg/ml), a process obtained by inversion and flotation of a coverslip onto the layer of buoyant adipocytes.

Rhodamine 123 staining. For primary adipocytes, the nucleus nub is routinely used as a morphological indicator to distinguish between adipocytes and fat droplets; however, to further aid identification, adipocytes were loaded with Rhodamine 123 (Rh-123, 10–20 μg/ml for 5 min in the dark at 22°C; Sigma), illuminated with an excitation wavelength of 450–490 nm, and viewed with a 510-nm long-pass emission filter (Zeiss filter Set 10).

3T3-L1 adipocyte culture. Cells in culture were kept at 37°C in a humidified atmosphere of 5% CO_2-95% air. 3T3-L1 fibroblasts were cultured in maintenance medium comprising Dulbecco's modified Eagle medium (DMEM) supplemented with 10% (vol/vol) newborn calf serum (NCS, Sigma N4637), 1% (vol/vol) antibiotic-antimycotic mix (Sigma A5955), 0.5% (vol/vol) gentamicin (Sigma G1272), and 2 mM L-glutamine. 3T3-L1 fibroblasts were grown in T75 flasks to 60% confluence prior to a 1:3 split twice a week.

For differentiation, cells were seeded in 35-mm culture dishes (Corning) and grown to confluence. Two days postconfluence, differentiation was initiated by incubation for 2 days in a differentiation medium: the maintenance medium but with fetal calf serum (10% vol/vol) instead of NCS, supplemented with 1 μg/ml porcine insulin, 0.5 mM 1-methyl-3-(2-methylpropyl)-7H-purine-2,6-dione (IBMX), and 0.25 μM dexamethasone. After that, the cells were incubated for a further 2 days in the differentiation medium but without dexamethasone and IBMX. Finally, the differentiated cells were maintained up to 5 days in the differentiation medium but with no supplements.

3T3-L1 oil red O hematoxylin counterstain. To confirm the presence and accumulation of lipid droplets following cell differentiation, we used Oil red O and hematoxylin counterstaining. Cells were washed with phosphate-buffered saline and then fixed in 10% (vol/vol) formalin. Oil drops were then stained by incubation in 2 mg/ml Oil red O in 60% (vol/vol) isopropanol. To visualize the nuclei, cells were counterstained with hematoxylin. Cells were observed and images taken using a phase contrast microscope at ×10 magnification.

Electrophysiology. For electrophysiology standard patch-clamp methods were used.

PERFORATED PATCH STUDY OF PLASMA MEMBRANE POTENTIAL. Membrane potential measurements were made using the perforated patch configuration of the whole cell patch clamp technique in current clamp mode. This technique has the advantage over conventional whole cell in that it maintains cellular metabolism and intracellular ionic composition, prevents ion channel rundown, and imparts little or no osmotic or shear stress on the studied cell (42). The pipette solution comprised (in mM): 76 K_2SO_4, 10 KCl, 10 NaCl, 55 sucrose, and 10 HEPES (pH 7.4 with NaOH). For perforation, pipettes were backfilled with a solution that also contained 0.1 μg/ml of the polyene antibiotic amphotericin. Perforation was considered adequate when the series resistance (Rs) was stable and less than 35 MΩ as determined by electronic compensation. For the 3T3-L1 adipocytes, Rs and cell capacitance were 32 ± 1 MΩ and 15.6 ± 13.9 pF (n = 100), respectively. Unfortunately, due to the large diameters of the primary adipocytes measured in these experiments as 75.2 ± 1.3 μm (n = 47), their cell capacitance could not be compensated by the amplifier (Axopatch 1D; Axon Instruments, Molecular Devices).

The input resistance (R_{in}) of the cells was monitored by the steady-state change in membrane potential (ΔVm) in response to steps of injected current (ΔI) of up to ± 40 pA applied for 0.1–20 s duration (12). R_{in} was calculated as the slope of the relationship between ΔVm and ΔI at *V*m. Cells with *V*m's depolarized to −10 mV were excluded from the analyses to prevent bias from leaky or damaged cells as also indicated by a low R_{in} values <100 MΩ.

CELL-ATTACHED STUDY OF SINGLE ION CHANNEL ACTIVITY. To investigate the properties of the ion channels responsible for *V*m, cell-attached patch clamp experiments were performed. To reduce electrical capacitance and improve noise, pipettes were coated at their tips with dental wax (Sticky Wax, Kerr). To maximize discovery of either Cl^- or NS ion channels, the pipette solution comprised (in mM) 140 KCl, 1.2 $MgCl_2$, 2.6 $CaCl_2$, and 10 HEPES (pH 7.4 with NaOH; 147 mM Cl^-). Pipettes had resistances of 3–5 MΩ. Membrane currents were recorded with an Axopatch 1D patch clamp amplifier (Axon instruments, Molecular Devices), filtered by an 8-pole Bessel filter at 0.5–2 KHz, and digitized at 5 KHz. Since most patches had a high level of channel activity, often with channel substates, single-channel amplitudes were measured by cursors with the median amplitude used for further analyses to overcome misclassification of temporally coincident openings. *V*oltage dependency of channel-open probability was estimated from all-point histograms. Inward currents are displayed as downward deflections by convention and potentials as membrane potential: $V\text{m} = V\text{r} - V\text{p}$, where *V*r is the resting membrane potential (assumed to be −30 mV) and *V*p the pipette voltage.

Intracellular Ca^{2+} imaging and analyses. The concentration of intracellular Ca^{2+} ($[Ca^{2+}]_i$) was monitored with Fluo 4 using standard epifluorescent imaging techniques. Adipocytes were loaded with dye by incubation in Hank's solution containing 1 μm Fluo 4-AM for 30 min in the dark at 21–23°C. Loaded cells were imaged using an inverted Axiovert 135T*V* microscope fitted with a ×20 FLUO objective (Carl Zeiss, Welwyn Garden City, UK). To monitor $[Ca^{2+}]_i$, cells were continuously illuminated at an excitation wavelength of 450–490 nm. The emitted light was bandpass filtered at 515–565 nm and

the signal detected using a Photonics Science ISIS camera with image intensification. Images were captured at 1 Hz with an 8-bit frame grabber (DT3155; Data Translation, Basingstoke, UK) and Imaging Workbench software (Indec Biosystems, Santa Clara, CA). For image analysis, a region of interest (ROI) was drawn around each cell, the background fluorescence subtracted, and the time course of its mean fluorescent intensity calculated. For some experiments, the fluorescence changes were calibrated by a two-point method: the maximum fluorescence (Fmax), determined by permeabilization of the cells with Triton X-100 (0.0125–0.1% vol/vol) was followed by perifusion of 10 mM EGTA to determine Fmin, the minimum fluorescence. To calculate $[Ca^{2+}]_i$, we used the following equation:

$$\left[Ca^{2+}\right]_i = K_d \times \frac{(F - F_{min})}{(F_{max} - F)}$$

where F is the background corrected fluorescence, and K_d is the dissociation constant of Fluo 4 (345 nM, Molecular Probes). For other experiments, fluorescence changes were left uncalibrated, with basal values taken as 100%. Adipocytes were perifused for at least 10 min before experimental intervention, with the time-averaged fluorescence intensity over this period taken as the basal level. We assumed that the dye was predominantly cytosolic in location.

Solutions. All experiments were performed under continuous perifusion in a HEPES-buffered Hank's solution that contained (in mM): 10 glucose, 138 NaCl, 4.2 $NaHCO_3$, 1.2 NaH_2PO_4, 5.6 KCl, 1.2 $MgCl_2$, 2.6 $CaCl_2$, 10 HEPES (pH 7.4 with NaOH), and 0.01% (wt/vol) fatty acid-free bovine serum albumin (BSA) at 32°C for perforated patch (the highest temperature at which stability was maintained), at room temperature (22–25°C) for single-channel recording (to slow gating kinetics and aid comparison with previously published biophysical data), and at 28°C for Ca^{2+} imaging (to limit the dye extrusion that occurred at higher temperatures). For the Li^+ experiments, 138 mM NaCl in the Hank's solution was replaced with 138 mM LiCl, whereas for the I^- experiments 138 mM NaCl was replaced with 138 mM NaI. In the ion substitution experiments, we corrected for the liquid junction potential (LJP) change that occurs at the reference potential. LJPs were measured experimentally following the methods as detailed in Smith et al. (43), and *V*m was adjusted accordingly. Osmolarities were measured in triplicate with a Roebling MicroOsmometer 12 (Camlab, Cambridge, UK).

Drugs and reagents. All drugs and reagents were obtained from Sigma. The relevant vehicles used for the drugs used are given in the results.

Statistical analyses. Analyses were performed using Origin software with bespoke scripts written in Labtalk (OriginLab).

All datasets were tested for normality with the D'Agostino and Pearson omnibus normality test. Statistical analysis was performed using Graphpad PRISM v. 6 (San Diego, CA), and the statistical test used is given in the text. Data are given in the text either as means ± SE or median with 5–95% confidence intervals (CI), with *n* the number of determinations. To show the range and distribution of values obtained, data are expressed in the figures as box and whisker representations, which show the median, interquartile range, and 5 and 95% CIs. The fitting of equations to the data used a least squares algorithm as supplied with PRISM. Statistical significance is defined as $P < 0.05$ and is flagged as * in graphics, ** when $P < 0.01$, or *** when $P < 0.001$.

RESULTS AND DISCUSSION

Identification of differentiated 3T3-L1 and primary adipocytes. Figure 1 shows representative images of 3T3 fibroblasts both prior to and at various stages of the differentiation process. Differentiation of 3T3-L1 fibroblasts to adipocytes is characterized by the accumulation of lipid droplets, clearly visible in some cells by the presence of stain (Fig. 1*B*). As the cells accumulate lipid, they become less flat and adopt a more rounded shape (Fig. 1*C*). Our differentiated 3T3-L1 adipocytes clearly adopted an appearance that is similar, but not identical, to that of the mature adipocytes (20, 21). 3T3-L1 fibroblasts at an intermediate stage of differentiation show multiple lipid droplets and a centralized nucleus. Fully differentiated 3T3-L1 adipocytes are spherical and contain a singular coalesced fat droplet (Fig. 1*C*, black arrows). Some cells within the population failed to differentiate (Fig. 1*C*), a previously noted phenomenon (21). Only fully differentiated single adipocytes were selected for electrophysiological study.

Figure 2 illustrates a typical pattern of fluorescence observed for primary adipocytes loaded with Rh-123. In this particular field, four of five of the adipocytes viewed were evenly loaded with dye and were considered suitable for patch clamp. The fifth cell was excessively fluorescent; such cells were occasionally observed, the reason for which was not explored and they were not considered for patch clamp.

Resting membrane potential of adipocytes. Both the primary and the differentiated 3T3-L1 adipocytes had median *V*m values that were not significantly different from each other at −31 mV (−32 to −27 95% CI, $n = 95$) and −28 mV (−30 to −24 95% CI, $n = 87$), respectively ($P > 0.05$, Mann-Whitney; Fig. 3), data that suggest that under resting conditions the plasma membranes of these two cell types possess common ion

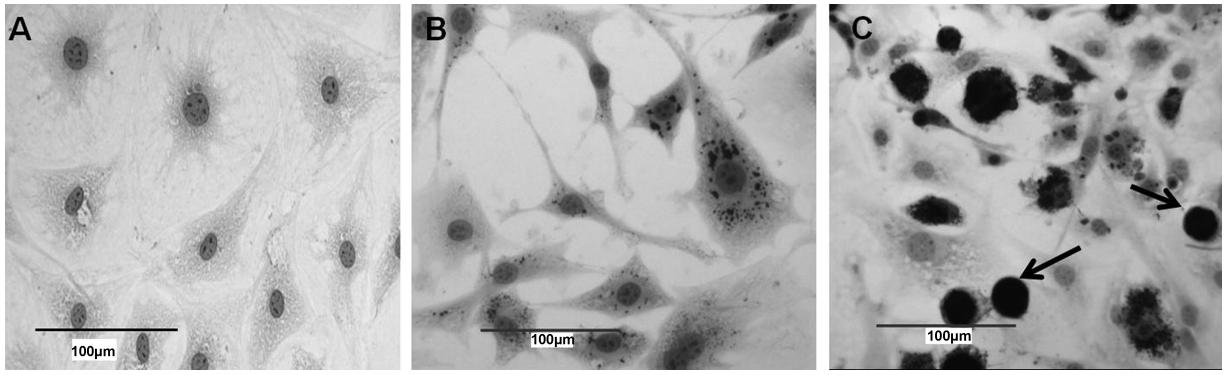

Fig. 1. Identification of 3T3-L1 adipocytes. Representative images of 3T3 fibroblasts at various stages of differentiation into adipocytes, stained with Oil red O and hematoxylin counterstain. *A*: undifferentiated cells. *B*: 96 h post-onset of differentiation process. Note that some cells now have fat droplets. *C*: post-completion of the differentiation protocol. Note the heterogeneous cell population of predominantly 3T3-L1 adipocytes with coalesced fat droplets (black arrow), but also a few undifferentiated 3T3 fibroblasts still exist. Black arrows indicate differentiated adipocytes. Scale bar, 100 μm.

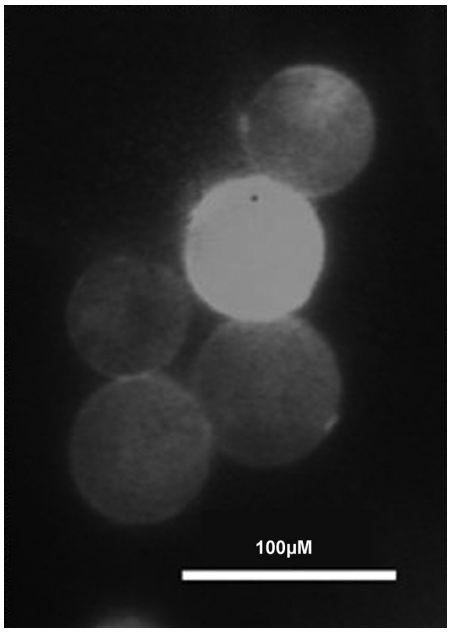

Fig. 2. Identification of primary adipocytes. Representative grayscale fluorescent image of primary adipocytes loaded with Rh-123. Although the degree of fluorescence is quite variable, in the majority of cases a clear outline of the plasma membrane can be discerned, with a slightly brighter plaque region indicative of the nuclear knob. Since fat droplets fail to fluoresce, they are not visible.

transport properties. The *V*m for the primary and differentiated 3T3-L1 adipocytes share a similar, negatively skewed frequency distribution (Fig. 3A), with median values almost identical to their mean values at -32.1 ± 1.2 and -28.8 ± 1.2 mV, respectively (Fig. 3*B*). The values of *V*m reported here, using the perforated patch clamp technique, compare very favorably with those previously reported for adipocytes from rat epididymal fat pads measured with other techniques (Table 1), being almost identical to that directly measured in white fat adipocytes with sharp electrodes (-34 mV, 39) or identified isolated adipocytes with whole cell patch clamp (-30 mV, 28), as well as that estimated from the passive distribution of Cl^- (-29 mV) based on an intracellular Cl^- concentration, $[Cl^-]_i$, of 43 mM estimated from $^{36}Cl^-$ efflux studies (34). Although, cell damage and current leakage across the pipette-cell seal may explain the spread of *V*m toward depolarized values, in order to account for the more hyperpolarized *V*m values, additional mechanisms are sought such as variation in ion permeability or intracellular ion concentration. Since the primary adipocytes had a resting *V*m distribution similar to that of the 3T3-L1 adipocytes, the underlying biophysical mechanisms are likely to be common to both cell types. Furthermore, the similar distribution of *V*m values between the two cell types excludes phenotypic heterogeneity as a source of variation in the primary cell data.

Input resistance of adipocytes and its relationship to cell size. Figure 4*A* shows representative measurements of *V*m and R_{in} in a primary adipocyte under normal, control conditions and after equimolar substitution of 138 mM bath Cl^- with I^-. The primary adipocytes had plasma membrane time constants in excess of 100 ms, values consistent with their large surface area (Fig. 4*B*). R_{in} varied with the ionic composition of the bath (Fig. 4*B*), a phenomenon explored later. Figure 4*C* illustrates that, under control conditions, both primary fat cells and differentiated 3T3-L1 adipocytes had similar median R_{in} at 0.6 GΩ (0.42 to 0.72 95% CI, $n = 40$) and 0.64 GΩ (0.37 to 0.78 95% CI, $n = 38$), respectively ($P > 0.95$, Mann-Whitney). These values of R_{in} are far larger than that previously reported with sharp electrodes (0.3 GΩ, 39) but similar to those measured with standard whole cell patch clamp (~1 GΩ, 28).

Given that primary adipocytes, assumed to be perfect spheres, had a significantly larger cell surface area at $17{,}700 \pm 613$ μm^2 ($n = 47$) than 3T3-L1 adipocytes, at $4{,}190 \pm 500$ μm^2 ($n = 24$, $P < 0.001$, Mann-Whitney), suggests that primary adipocytes have one-quarter of the channel density as the cell line. In the primary adipocytes, R_{in} was negatively (Spearman $r = -0.4$, $P < 0.01$) correlated with cell diameter (Fig. 4*D*), data that suggest that larger adipocytes possess greater ion channel activity. *V*m was negatively (Spearman $r = -0.48$, $P < 0.001$) correlated to R_{in} (Fig. 4*E*). Since R_{in} is clearly related to cell size (Fig. 4*D*) and *V*m (Fig. 4*E*), it could be inferred that larger cells may possess a more depolarized *V*m, although this did not seem to be the case for 46 cells for which cell diameter was measured, where Fig. 4*F* clearly shows that the magnitude of *V*m appears to be independent of cell diameter, even though their R_{in} ($n = 31$) was still negatively correlated with cell diameter (Spearman $r = -0.42$, $P < 0.01$) and *V*m (Spearman $r = -0.5$, $P < 0.01$). Due to the uncertainty of the exact cell geometry (Fig. 1*C*) of the differentiated 3T3-L1 adipocytes, they were not subjected to the above analyses.

Ionic dependence of membrane potential. Figure 5 shows the effect of extracellular ion composition on *V*m for both types of adipocytes. Since K^+ ions have a major role to play in the

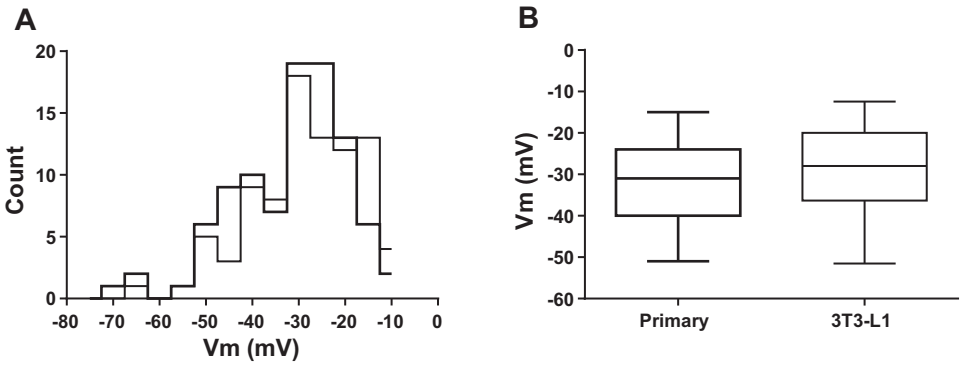

Fig. 3. Distribution of membrane potential in primary and 3T3-L1 adipocytes. *A*: distribution of membrane potential (*V*m), measured using the perforated patch clamp technique for primary adipocytes (thick line) and 3T3-L1 adipocytes (thin line). Note their striking similarity in shape. *B*: box and whisker plot of *V*m for primary (thick line, $n = 95$) and 3T3-L1 adipocytes (thin line, $n = 87$) for data shown in *A*.

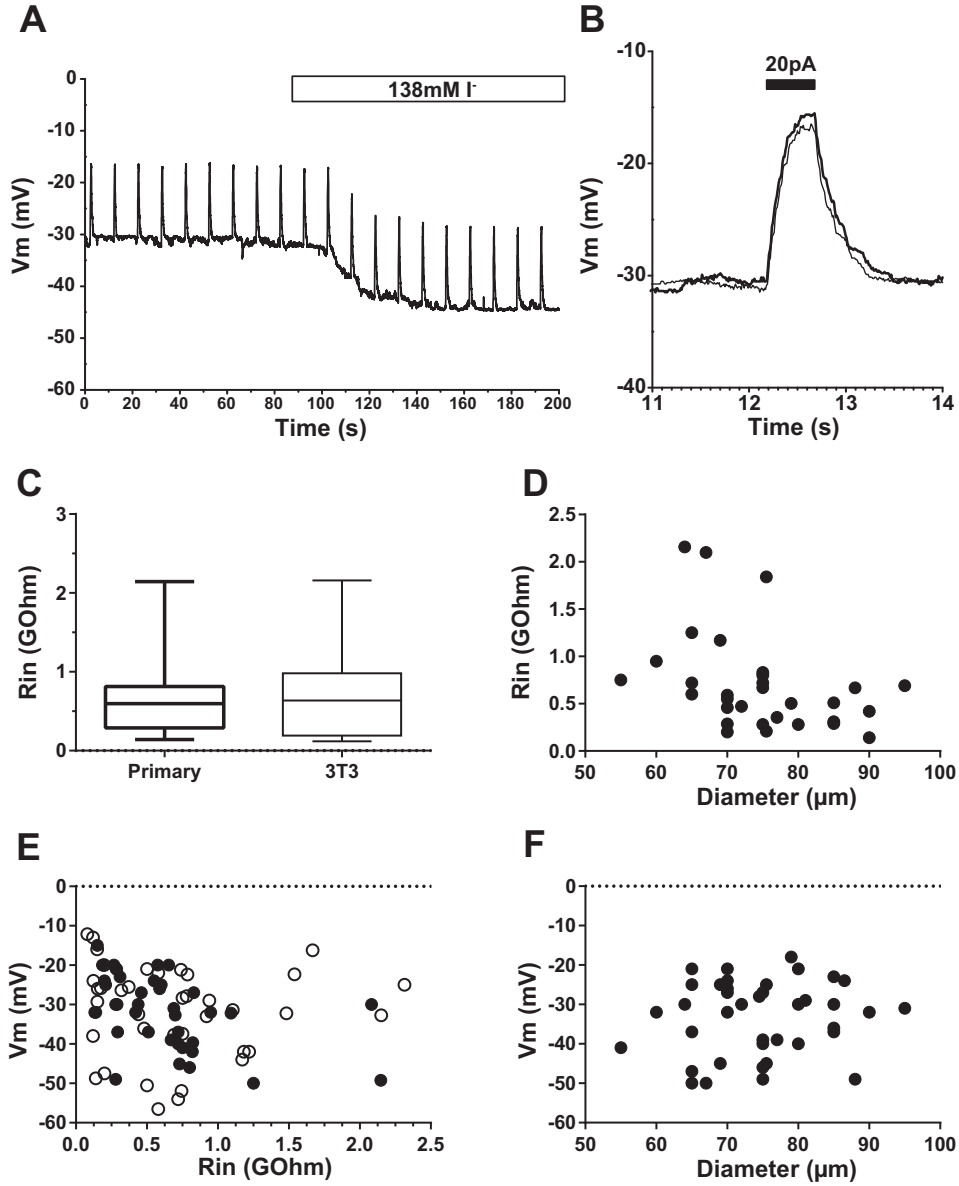

Fig. 4. Measurement of Input resistance (R_{in}) and *Vm* in primary and 3T3-L1 adipocytes. *A*: *Vm* measured using the perforated patch clamp technique for a primary adipocyte in response to equimolar substitution of 138 mM bath Cl^- with I^-. Upward, positive deflections are *Vm* changes to a +20-pA current injection of 500 ms duration applied at frequency of 0.1 Hz used to calculate R_{in}. *B*: expansion of representative *Vm* deflections due to a +20-pA current injection under control (thick line) and I^- substitution (thin line) conditions, both of which show the slow charging time course of the adipocyte plasma membrane. *C*: box and whisker plot of R_{in} for primary (thick line, $n = 41$) and 3T3-L1 adipocytes (thin line, $n = 38$) for data shown in *E*. *D*: negative correlation between R_{in} and primary adipocyte diameter ($P < 0.01$). *E*: plot of *Vm* against R_{in} for primary (●) and differentiated 3T3-L1 adipocytes (□). *F*: lack of correlation between *Vm* (●) and primary adipocyte diameter, data as in *D*.

control of membrane potential for many classes of cell and also have been shown to affect both *Vm* (6, 7) and $[Ca^{2+}]_i$ (36, 38) of white fat tissue, the effect of this ion on the membrane potential of adipocytes was first to be tested.

Elevation of the extracellular concentration of potassium ions ($[K^+]_o$) from 5.6 to 50 mM by equimolar substitution of bath Na^+ had no significant effect (paired *t*-test) on the membrane potential of either type of adipocyte, with a mean difference of <1 mV in both cases (Fig. 5, *A* and *B*) (Friedman's test), although others have reported the *Vm* of white fat tissue to be affected by changes in extracellular K^+ (6, 7), an observation suggested to be limited to rats weighing less than 215 g (6), which generally have smaller adipocytes (14). Although this may be proposed as the reason why we failed to see an effect of K^+ on *Vm*, our data refute this idea, since we observed no correlation between *Vm* and adipocyte diameter (Fig. 4*F*); furthermore, no such relationship was observed in the differentiated 3T3-L1 adipocytes, which were variable in size. One possible reason for this discrepancy in the K^+ ionic dependency of adipocyte *Vm*, is that in our study isolated adipocytes were clearly identified as such, whereas in previous studies of the ionic dependency of *Vm* sharp electrodes were impaled blindly into white fat explants, where it was assumed that *Vm* was recorded from adipocytes. This is a pertinent point, since only a narrow band of cytoplasm circumnavigates the lipid droplet (11, 49), whereas other cells of the adipose tissue, such as smooth muscle and endothelia of its vasculature, being larger, have a higher likelihood of actual impalement and have *Vm* values quite similar to those reported for identified adipocytes; for example, the resting membrane potential of smooth muscle myocytes from a variety of arterial tissues range from −32 mV in pulmonary (3) to −39 mV in renal (8), whereas the resting *Vm* for endothelial cells range from −26 mV from pulmonary artery (52) to −43 mV from aorta (9). Another possible reason for this discrepancy is that in previously published work (6), although not explicitly given, the

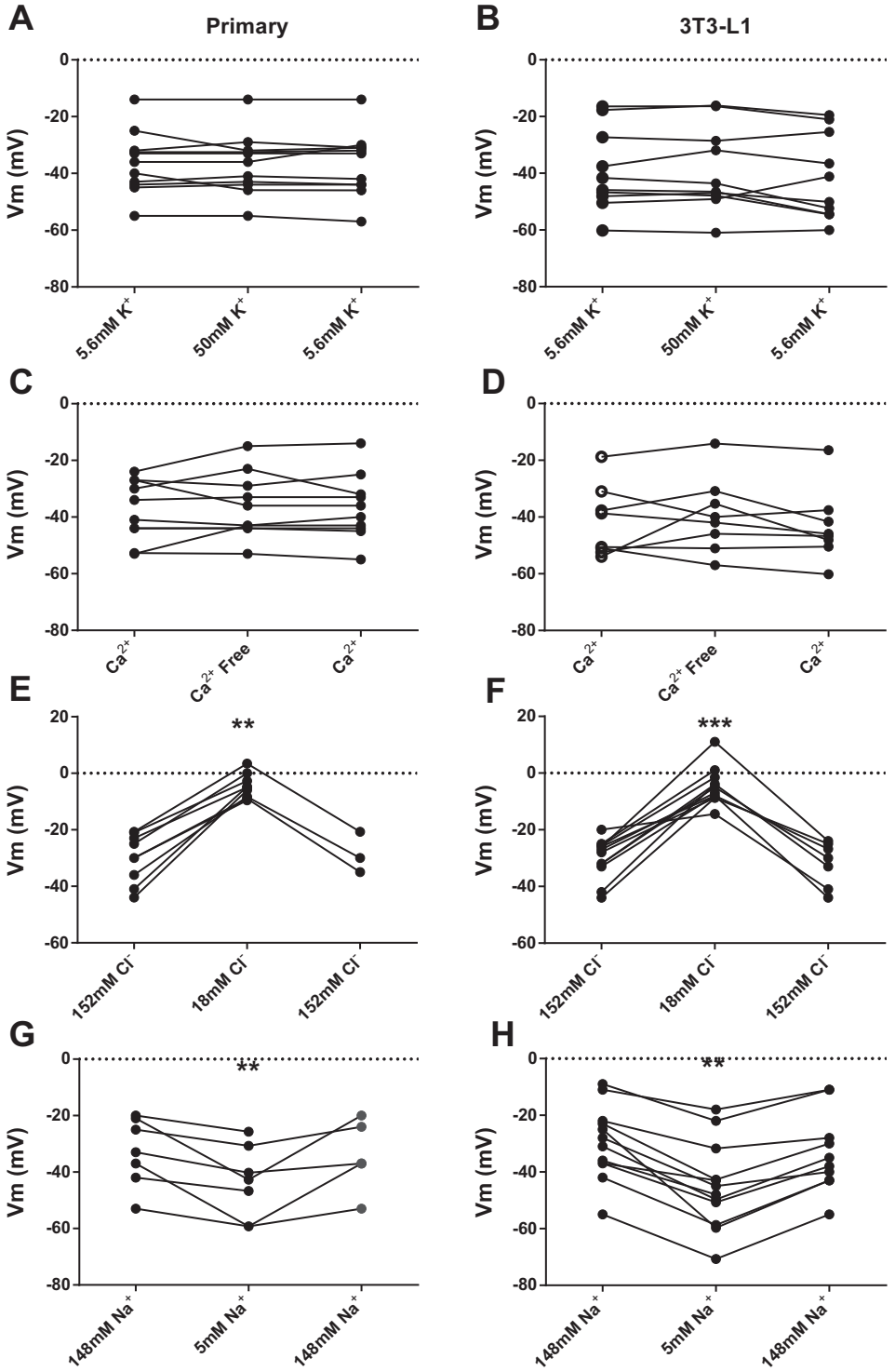

Fig. 5. Effect of different ions on the membrane potential of primary and 3T3-L1 adipocytes. Effect of changes in extracellular ion concentrations as indicated on the *V*m of primary adipocytes (*left*) and 3T3-L1 adipocytes (*right*). *V*alues represent individual measurement of *V*m once a steady-state value was reached after bath exchange. Statistical significance was determined relative to initial ionic conditions via Wilcoxon. The number of experiments is explicitly represented by the number of before-after lines: 7–12 for each experimental paradigm.

authors state the composition of their high $[K^+]_o$ solutions were the same as those used by Hodgkin and Horowicz (23). Inspection of these original methods (23) reveals that these contain varying or nominal $[Cl^-]_o$. In a sequential study (7), this problem was resolved, since $Cl^-]_o$ was given; moreover, the same study went on to demonstrate that Cl^- did indeed contribute to adipocyte *V*m, an anion we later show to be predominant in the control of adipocyte *V*m.

In fact, many other factors could pervade in cell suspensions and intact tissue that may affect ion channel behavior and are not present in our sanitized, perifused, single isolated cell paradigm, such as paracrine modulation and physical interaction.

As we (38) have previously demonstrated that white fat adipocytes have a background Ca^{2+} influx pathway, the effect of removal of this ion by substitution with equimolar Mg^{2+}

was tested; no significant effect on *Vm* was detected (Fig. 5, *C* and *D*). These results indicate that the plasma membrane of both types of adipocyte do not appear to have a selective permeability to either K^+ or Ca^{2+} ions or, if they do, the contribution of these ions to *Vm* is so small that our experimental paradigm does not have the statistical power to detect it. Since white fat adipocytes have a negative membrane potential that appears to be independent of the concentration of $[K^+]_o$, our data suggest that *Vm* must be predominantly controlled by the passive distribution of Cl^- ions. This hypothesis was tested by equimolar substitution of 134 mM bath Cl^- with the gluconate anion (Fig. 4). After correction for the change in LJP at the reference electrode (8.3 mV), a reduction in extracellular Cl^- from 152 mM (300 ± 2.7 mOsm) to 18 mM (282 ± 2.3 mOsm) resulted in a significant and reversible depolarization in *Vm* of +24 mV (18 to 36 mV, 95% CI, $P < 0.002$, Wilcoxon) and +26 mV (20 to 28 mV, 95% CI, $P < 0.0002$, Wilcoxon) for primary and 3T3-L1 differentiated adipocytes, respectively or, for pooled data, +25 mV (20 to 28 mV, 95% CI, $P < 0.0001$, Wilcoxon, $n = 21$): from −28 mV (−33 to −25 mV, 95% CI) to −4.7 mV (−2.7 to −8.3 mV, 95% CI). These data are consistent with the work of Beigelman and Shu (7), who demonstrated that the *Vm* of white fat adipocyte has a Cl^--dependent component, as well as that of Hales and Perry (36), who suggest that *Vm* is solely Nernstian in behavior for Cl^- and is given by the diffusion potential for Cl^-: E_{Cl}. If the latter is true, then we estimate from our values of *Vm* that $[Cl^-]_i$ is 50 ± 3 mM ($n = 21$). However, the fact that on reduction of $[Cl^-]_o$ *Vm* depolarized to a value that was significantly different from the *Vm* predicted (+26.0 ± 1.6 mV) using our $[Cl^-]_i$ estimate and a Nernstian behavior for Cl^- ($P < 0.001$, paired *t*-test) implies that other ionic permeabilities must also be involved in the generation of adipocyte *Vm*.

To test for the contribution of monovalent cation permeability to the generation of *Vm*, the majority of extracellular monovalent cations were removed via equimolar substitution of 138 mM bath Na^+ with $NMDG^+$ (*N*-methyl-D-glucamine; 291 ± 0.3 mOsm), a large organic cation considered impermeant through monovalent cation channels (1). This ionic substitution resulted in a significant and reversible hyperpolarization in the *Vm* for both primary and 3T3-L1 differentiated adipocytes of −7.2 mV (−28.2 to −4.7 mV, 95% CI, $P < 0.008$, Wilcoxon) and −16.7 mV (−34.7 to −9.7 mV, 95% CI, $P < 0.008$, Wilcoxon), respectively (Fig. 4, *G* and *H*). Since the magnitude of hyperpolarization was insignificantly different between the two cell types ($P = 0.45$, Mann-Whitney), data were pooled to give −16.2 mV (−21.7 to −7.2 mV, 95% CI, $P < 0.0001$, Wilcoxon). The fact that removal of Na^+ but not its substitution with K^+ affected *Vm* supports the existence of nonselective, monovalent cation permeability, P_{NS}, in the control of adipocyte *Vm* with a P_K/P_{Na} ratio of ~1.

Exploration of Cl^- dependency of Vm. Since Cl^- appeared to be the predominant ion that controls the membrane potential for both types of adipocytes, the dependency of *Vm* on the external chloride concentration, $[Cl^-]_o$, was explored further. Figure 6*A* shows typical changes in *Vm* recorded from a 3T3-L1 differentiated adipocyte in response to eight consecutive decrements in $[Cl^-]_o$. A new stable *Vm* was reached within 1 min of each solution change. Complete recovery of the original resting value of *Vm* was achieved on return to 152 mM $[Cl^-]_o$. The Goldman constant field model (22) was used to quantitate the relationship between ion concentration and *Vm* via the Goldman-Hodgkin-Katz membrane potential equation (GHK), with the assumption that electrogenic processes did not contribute to the generation of *Vm*:

$$V_m = -\frac{RT}{F} ln\left[\frac{P_{NS}[K^+]_i + P_{NS}[Na^+]_i + P_{Cl}[Cl^-]_o}{P_{NS}[K^+]_o + P_{NS}[Na^+]_o + P_{Cl}[Cl^-]_i}\right]$$

where *R* is the universal gas constant (8.314 $J \cdot mol^{-1} \cdot K^{-1}$), T the absolute temperature (305K) and *F*, Faraday constant (96.4 kC/mol). $[K^+]_i$, $[Na^+]_i$, and $[Cl^-]_i$ are the intracellular and $[K^+]_o$, $[Na^+]_o$, and $[Cl^-]_o$ the extracellular concentrations for potassium, sodium, and chloride, respectively. P_{NS} is the monovalent cation permeability (nonselective) and P_{Cl} is the permeability to Cl^-. If we assume no contribution from divalent cations and the major passive permeability for monovalent cations is P_{NS}, then the intracellular and extracellular cations can be lumped together and the relative permeabilities of Cl^- and monovalent cations, P_{Cl}/P_{NS}, defined as *Alpha*. For $[K^+]_i + [Na^+]_i$, we used 152.6 mM, 134 mM for $[K^+]_i$, and 18.6 mM for $[Na^+]_i$, as determined from the radioisotope efflux studies of Perry and Hales (34). A similar value of 150 mM is argued by Thoresteinsson et al. (47), who independently measured $[K^+]_i$ and $[Na^+]_i$ in white fat cells with radioisotopes, as well as that of 152 mM calculated from the sum of $[K^+]_i$ and $[Na^+]_i$ measured with ion-sensitive microelectrodes in white fat adipocytes by Stark et al. (44). The value of $[Cl^-]_i$ given by Perry and Hales (34) is the mean from a cell population study, whereas here individual cells are being investigated that reveal cell-to-cell variation. To account for the latter, we varied both *Alpha* and $[Cl^-]_i$ during fitting GHK to our data. To account for any passive permeability of the gluconate anion though the chloride permeability pathway, $[Cl^-]_o$ was substituted by:

$$[Cl^-]_o + Delta\,[Gluc^-]_o$$

where $[Gluc^-]_o$ is the extracellular concentration of gluconate and *Delta* its relative permeability to that of chloride: P_{Gluc}/P_{Cl}. For $[K^+]_o$, $[Na^+]_o$, and $[Cl^-]_o$ we used 5.6, 148, and 152 mM, respectively, values calculated from the formulation of our extracellular Hanks' solution. For all calculations we used ion concentrations and not their activities.

Representative fits of GHK to the *Vm* data for the primary and 3T3 adipocytes are shown in Fig. 6*B*. Also shown are the range of *Alpha* (Fig. 6*E*) and $[Cl^-]_i$ (Fig. 6*F*), values calculated for the two cell types when either $[Cl^-]_o$ or $[Na^+]_o$ was singularly varied. Since the values obtained for both *Alpha* and $[Cl^-]_i$ were statistically independent (Kruskall-Wallis) of cell type and experimental paradigm, their values were pooled. Pooled values for *Alpha* were 4.8 (3.6 to 8.4 95% CI, $n = 36$) and 27 ± 2.5 mM ($n = 36$) for $[Cl^-]_i$, the latter significantly smaller ($P < 0.001$ one-sample *t*-test) than the 43 mM estimated from $^{36}Cl^-$ efflux data (34). *Vm* was best fitted with *Delta* values of 0.129 and 0.144 for primary and 3T3 adipocytes, respectively.

Consistent with the dominance of Cl^- in the control of *Vm*, the input resistance (R_{in}) significantly increased ($P = 0.04$, paired *t*-test, $n = 6$) from 0.78 ± 0.16 GΩ to 1.52 ± 0.32 GΩ with the decrease in $[Cl^-]_o$. If we assume that the increase in R_{in} (0.74 ± 0.27 GΩ) arose solely due to the decrease in the concentration of the permeating ion Cl^-, then the change in membrane conductance, ignoring the contribution by glu-

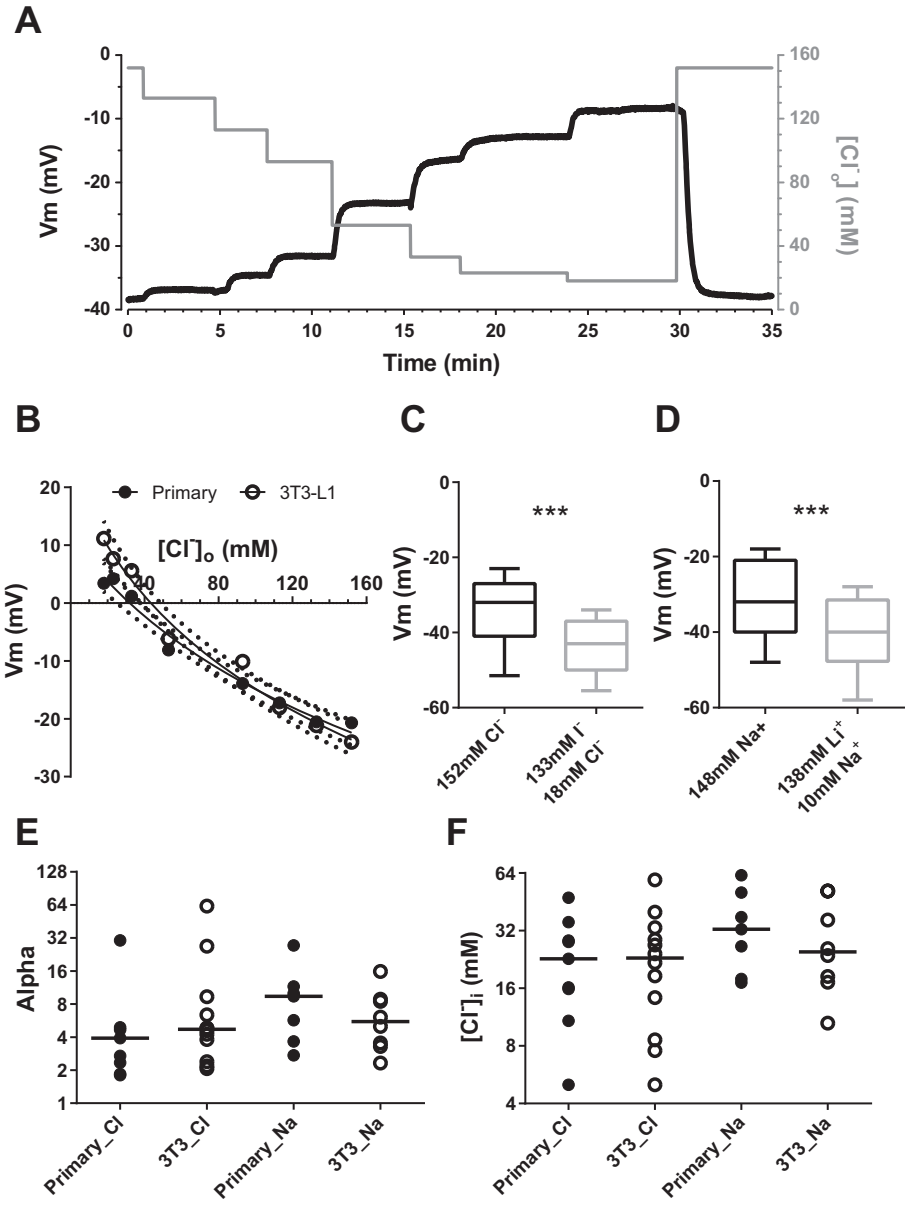

Fig. 6. Determination of the permeability ratio *Alpha* for primary and 3T3-L1 adipocytes. *A*: *Vm* (thick black line) in response to changes in bath extracellular Cl^- concentration $[Cl^-]_o$ (thin gray line), recorded from a 3T3-L1 adipocyte. *B*: representative plots of the membrane potential determined at different $[Cl^-]_o$ for a primary (●) and differentiated 3T3-L1 adipocyte (○). Solid lines are best fits to the Goldman-Hodgkin-Katz membrane potential equation (GHK) with *Alpha* values of 4.9 and 27, and $[Cl^-]_o$ of 48 and 59 mM for primary and differentiated 3T3-L1 cells, respectively. Dotted lines describe the 95% confidence intervals (CI) for respective fits. *C*: effect of substitution of 133 mM bath Cl^- with I^- on the *Vm* of primary adipocytes. *D*: effect of substitution of 138 mM bath Na^+ with Li^+ on the *Vm* of primary adipocytes. *E*: estimates of *Alpha*, the permeability ratio of P_{Cl}/P_{NS} determined from fits of the GHK when either $[Cl^-]_o$ or $[Na^+]_o$ was allowed to vary. *F*: estimates of $[Cl^-]_o$ from fits of the GHK equation to the dependency of *Vm* on either changes in $[Cl^-]_o$ (_Cl suffix) or $[Na^+]_o$ (_Na suffix) for the 2 types of adipocytes as indicated. Median values are given by solid horizontal bars.

conate, is given by $\Delta G = G_{Cl} - G_{Cl}'$, where G_{Cl} and G_{Cl}' are the chloride conductances in 152 mM and 18 mM extracellular Cl^-, respectively. ΔG can be estimated from

$$\Delta G = \frac{R_{in} - R_{in}'}{R_{in}\,R_{in}'}$$

where R_{in} and R_{in}' are the input resistances measured in normal and low $[Cl^-]_o$, respectively; this gives an estimated ΔG of -1.18 ± 0.26 nS, or 0.058 ± 0.013 S m^{-2} for primary adipocytes considered as a sphere of diameter ~80 μm.

With the Goldman constant field model, the membrane conductance for any ion, G_j, is obtained by differentiation of the Goldman flux equation with respect to *Vm* (13):

$$G_j = P_j \frac{-az_jF}{(1-\exp[aE])^2}\left[(C_0 - C_i)(\exp[aE]) + (C_o - C_i\exp[aE])(1-\exp[aE])\right]$$

where P_j is the passive permeability for ion *j*, C_o and C_i are the respective extracellular and intracellular concentrations of ion *j*, $\alpha = z_jF/RT$ (z_j the valency of ion *j*), and E is the membrane potential. Since we know E, C_o, and C_i under two different extracellular Cl^- conditions, by using ΔG we estimate P_{Cl} as 0.364 nm/s with 27 mM $[Cl^-]_i$ or 0.345 nm/s with 43 mM $[Cl^-]_i$.

It is also possible to calculate the permeability to an ion from its efflux rate constant, if it is assumed to be totally passive in nature, by using the Goldman constant field model (22, 13):

$$P_j = k_j \frac{V}{A}\left[\frac{1}{aE}(1-\exp[-aE])\right]$$

where k_j is the efflux rate constant for ion *j* and *V*/A the volume of cell water to surface area ratio for a single cell. Since the cell volume of adipocytes is predominantly composed of the lipid droplet (11), it is necessary to know the percentage of the cell

volume that is occupied by water to gain an accurate estimate of *V*/A. The percentage of water content of adipocytes has been reported to be between 2.3% (19) and 2.75% (47). However, since this value is negatively correlated with rat weight and cell size (14), a revised value of ~2% was estimated for the mean *V* of 268 pl of our primary adipocytes. This gives a *V*/A of 0.26 μm, a volume manifested as the thin ring of cytoplasm of ~0.3 μm average thickness around the central lipid droplet (11, 49). Using k_{Cl} of 0.158 min^{-1} from Perry and Hales (34), P_{Cl} is calculated to be 0.4 nm/s, a value within 20% of those we estimate from the electrophysiological changes in R_{in} and *V*m.

In white fat adipocytes, $^{36}Cl^-$ efflux is observed to decrease with a reduction in extracellular anion concentration; these data were originally used to support the notion that ~30–40% of the $^{36}Cl^-$ efflux from adipocytes occurred by exchange with external anions (35). Such a result, however, can also be simply explained as due to a change in the electrochemical gradient for Cl^-, in particular the change in *V*m that occurs on removal of $[Cl^-]_o$. This idea can be checked by comparison of the predicted ratio of passive efflux rate constants with those actually measured. The expected passive efflux ratio (4) is given by

$$\frac{k_{j,1}}{k_{j,2}} = \frac{E_1\left(1 - \exp\left[-aE_2\right]\right)}{E_2\left(1 - \exp\left[-aE_2\right]\right)}$$

where $k_{j,1}/k_{j,2}$ is the expected ratio with membrane potentials E_1 and E_2 in low and normal $[Cl^-]_o$, respectively. From our *V*m data, we predict the $k_{j,1}/k_{j,2}$ ratio to be 0.65, which is similar to the ratio of 0.7 calculated from the actual $^{36}Cl^-$ efflux rate constants (0.157 and 0.110 min^{-1}) measured under similar experimental conditions by Perry and Hales (35). Consequently, our data support the notion that the P_{Cl} in adipocytes represents a predominantly passive diffusion pathway via ion channels rather than one mediated by anion exchange.

Our demonstration that white fat adipocytes have a *V*m that is predominantly dependent on P_{Cl} is contrary to previous suggestions that P_K is predominant in the control of adipocyte *V*m (6). Although we have already discussed this at length, the calculations above yield results that are entirely and internally consistent with our finding.

We observed a very negative spread of *V*m with 25% of all values (n = 182) hyperpolarized beyond −39 mV, and 18 values beyond −47mV (Fig. 3*A*). A *V*m solely Nernstian for Cl^-, i.e., with no P_{NS} component, based upon previously published (43 mM, 34) or even our own (27 mM) value of $[Cl^-]_i$ can muster maximum *V*m's of only −33 and −45 mV, respectively. These data suggest that in order to obtain the most negative of *V*m values (−72 mV) either those cells have a substantially lower $[Cl^-]_i$ than the population mean ~10 mM with little or no P_{NS}, or/and these cells have an extra P_K component that contributes to *V*m. Hyperpolarized adipocytes with an extra P_K component would be expected to exhibit increased and decreased *V*m responses to changes in $[K^+]_o$ and $[Cl^-]_o$, respectively; however, since neither was observed, the presence of a P_k to explain the more negative values of *V*m is unsupported.

During R_{in} measurement we assumed that the adipocytes had a large electrical space constant and reached isopotential within a few seconds of current injection. Since the cytoplasm exists as a thin 0.3-μm-thick submembrane sheet, due to internal resistance considerations, R_{in} and ΔG may be considered to be under- and overestimated, respectively (45). The fact that our estimate of P_{Cl}, determined from R_{in} and ΔG, was close to that obtained from radioisotope flux studies is strong evidence in support of the assumption of isopotential.

Effects of insulin and isoprenaline on membrane potential. Insulin and (nor)epinephrine are the two main modulators of adipocyte function. With this in mind, we sought to test whether they affected adipocyte *V*m. Figure 7 shows that perifusion of 100 nM insulin at 32°C did not affect the membrane potential of primary or of 3T3-L1 adipocytes. The

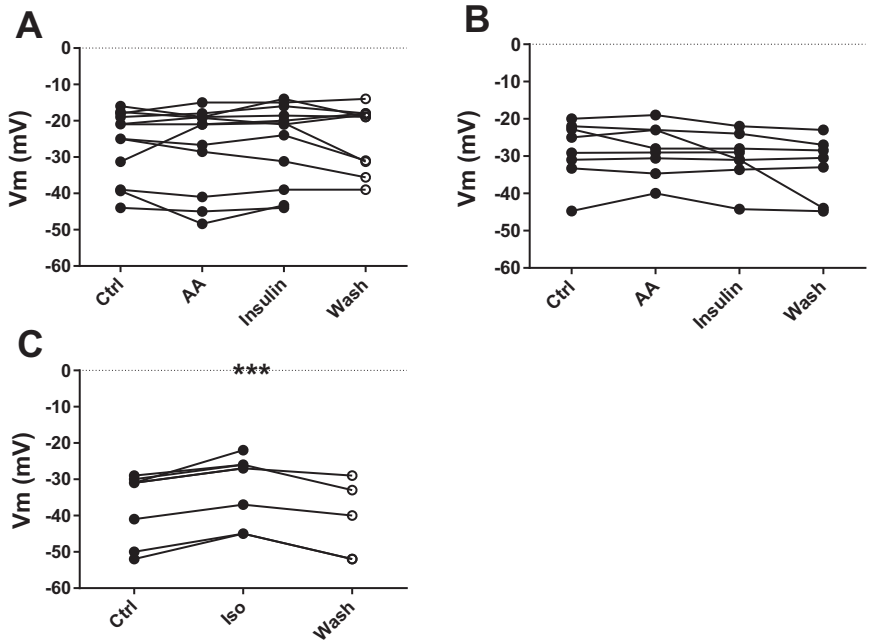

Fig. 7. Effects of insulin and isoprenaline on *V*m. Effect of 100 nM insulin on *V*m of primary (*A*) and 3T3-differentiated adipocytes (*B*). *C*: effect of 10 μM isoprenaline (iso), on the *V*m of 3T3-differentiated adipocytes. AA, acetic acid control. Statistical significance is relative to control (Student's paired *t*-test).

failure of insulin to affect *V*m or membrane permeability (*Alpha*) is supported by previous biophysical studies that also showed an absence of acute peptide effect on *V*m measured epididymal fat pad explants with sharp electrodes (5, 44) as well as $^{42}K^+$ efflux from isolated adipocytes (35). However, Beigelman and Hollander (5) report a depolarization of *V*m with insulin in adipocytes from young animals, whereas, conversely, Cheng et al. (10) reports that the peptide hyperpolarizes *V*m of white fat cells from similar aged animals. Overall, this body of evidence refutes an effect of the peptide on *V*m.

Perifusion of 10 μM isoprenaline, a β-adrenoceptor agonist, significantly and reversibly depolarized the plasma membrane by 5 ± 0.7 mV ($n = 8$, $P < 0.001$, Student's paired *t*-test; Fig. 7*C*). Furthermore, this was associated with a significant decrease in R_{in} from 0.35 MΩ (0.30–0.85, 95% CI) to 0.33 MΩ (0.23–0.79, 95% CI, $P < 0.05$, Wilcoxon test). The depolarization in *V*m produced by isoprenaline can be explained by a decrease in *Alpha* from 4.8 to 3.0 ($[Cl^-]_i = 27$ mM), as a result of either a decrease in P_{Cl} or an increase in P_{NS}, or both. However, since the change in *V*m was associated with a decrease in input resistance, an increase in P_{NS} is supported. Using the analytical approaches above, we estimate that the change in ΔG observed with isoprenaline is +0.0135 S/m^2 (0.0042 to 0.051, 95% CI): an increase in P_{NS} from 0.076 nm/s, calculated from *Alpha* (4.7) and P_{Cl} (0.49 nm/s) under control conditions, to 0.10 nm/s in the presence of the drug, which gives a new *Alpha* of 3.6, close to that estimated above to explain the change in *V*m observed with this drug. Perry and Hales (35) demonstrated that epinephrine increased cation ($^{42}K^+$) efflux, an event consistent with biophysical changes that we observe: an increase in cation permeability. However, the actual change in P_K associated with epinephrine, estimated from radioisotope efflux data, was 0.13 nm/s (35), 0.1 nm/s larger than the change in P_{NS} that we determined electrophysiologically: 0.03 nm/s. This is a finding that suggests that ~0.1 nm/s cation permeation is not mediated by ion channels but is probably due to ion exchange. Importantly, the same authors (35) also reported an increase in $^{36}Cl^-$ efflux with epinephrine, which we estimate from their data to be associated with an increase in P_{Cl} of 0.1 nm/s, a phenomenon apparently contradictory to that expected with our observed depolarization in *V*m. The nearly identical values for the increases in P_K and P_{Cl} that are unaccounted for electrophysiologically suggests that some form of electroneutral K-Cl cotransporter (COT/KCC) is activated in adipocytes with β-adrenoceptor activation, a phenomenon that is well established in many other cell types (2).

The ability of isoprenaline to depolarize *V*m is similar to that previously reported, an action also blocked by the nonselective β-adrenoceptor antagonist propranolol (10). Furthermore, using the cell-attached patch clamp technique, Ringer et al. (40) demonstrated a β_3-adrenoceptor-mediated activation of a nonselective cation channel on white fat adipocytes, an observation wholly consistent with the increase in nonselective cation permeability that we infer. The role of this phenomenon is unclear; it may be simply coincidental with β-adrenoceptor-mediated lipolysis, or alternatively, it may serve a role to regulate cell volume during the act of lipolysis.

Cell-attached single-channel studies. To characterize the identities of the ion channels responsible for the resting membrane potential of the adipocytes, the cell-attached configuration of the patch clamp technique was used. Figure 8*A* shows one type of single-channel current activity typical for that measured in 11 of 19 patches that possessed single-channel activity. At a *V*m of −90 mV, distinct inward-current single-channel activity was observed characterized by relatively long open states with occasional substates. The opening probability, NPo, was voltage independent over the *V*m range tested (Fig. 8*C*). The relationship between single-channel current amplitude and membrane potential, *i-V*, demonstrates outward rectification (Fig. 8*E*) with a single-channel slope conductance, γ, of 16 ± 1.3 pS and an extrapolated reversal potential, Rp, of −29 ± 1.6 mV ($n = 11$). The similarity of Rp to the estimated E_{Cl} of −32 ± 1.8 mV supports Cl^- as the predominant permeant ion species for this channel. To further characterize the single-channel *i-V* relationship, the data were fitted with the following form of the Goldman flux equation, assuming the intracellular and extracellular surface potentials were identical (43, 37):

$$i_j = P'_j \frac{-E(F_z)^2}{(1 - \exp[aE])}(C_o - C_i \exp[aE])$$

where i_j is the single-channel current amplitude and P'_j is the single-channel permeability for ion *j*. Since *E* (*V*m) and C_o (147 mM) are known, the *i-V* were fitted with a C_i and P'_{Cl} of 41 ± 3 mM and 7.1 ± 0.9 × 10^{-14} cm^3/s, respectively ($n = 5$). The close agreement between C_i and the measured values for $[Cl^-]_i$ further supports Cl^- as the permeant ionic species for these single-channel currents. Although γ and P'_{Cl} are about twice as large as those described for the CLC family and cystic fibrosis transmembrane regulator (CFTR) Cl^- channels recorded under similar conditions in recombinant cell models (16, 37, 46, 48), the observation of substates suggests that these adipocyte Cl^- channels may have a multimeric molecular identity or multiple configurations. Alternatively, they may be an adipocyte homolog of the volume-regulated anion channel (*V*RAC), which has similar biophysical properties to the channel we describe: an inward γ of 10–20 pS under similar ionic gradients, voltage-independent gating, and slow gating kinetics (32). Indeed, these channels may be the same as those responsible for the volume-sensing outward-rectifying (*V*SOR) chloride currents described in mature white fat adipocytes (24, 25).

In the other eight patches, single-channel currents similar in kinetics to those above were also observed (Fig. 8*B*); however, their inward slope conductance was significantly smaller at 9.8 ± 0.4 pS ($P < 0.002$, Student's *t*-test) with a significantly depolarized Rp of 8.9 ± 4.5 mV ($P < 0.0001$, Student's *t*-test; Fig. 8*F*). Moreover, they often possessed transitions between substates as well as noisy fluctuations in current amplitude that were greater than the unitary (sub)event (Fig. 8*B*). These, too, had a voltage-independent NPo (Fig. 8*D*). Although these properties are typical of those often observed for single-channel Cl^- currents (37, 47), the possession of an RP positive to 0 mV contradicts a Cl^- identity. It is possible that these channels represent a different mode of opening from the former ones described above, a change

possibility brought about by cell damage to give a depolarized and erroneous estimate of *V*r and Rp coupled with impairment of cellular signals that normally modulate channel gating. These channels were not characterized any further. We failed to see ion channel activity indicative of the nonselective ion channels with a γ of 25 pS, as previously described in white fat adipocytes by Ringer et al. (40).

Iodide permeability of the chloride channel. Since both the CFTR, a member of the ABC family of transporters (31), and the CLC familiy of chloride channels (46) have a far lower permeability to I^- than for the Cl^- anion, whereas the opposite is true for other Cl^- channels such as *V*SOR and *V*RAC (32), we tested the effect of substitution of bath Cl^- with I^- on the *V*m of primary adipocytes. Figure 4*A* shows that the substitution of 133 mM bath Cl^- with I^- (307 ± 4.2 mOsm) led to a stable and significant 9 ± 1.3 mV ($n = 11$) hyperpolarization ($P < 0.0001$, paired *t*-test) of *V*m (Fig. 6*C*). These data clearly show that primary adipocytes have a *V*m that is predominantly controlled by P_{Cl} with a greater ionic permeability to I^- compared with Cl^- and also dismisses a major role for either CFTR or CLC in the control of *V*m. Fitting the following form of the GHK equation to our data

$$Vm = -\frac{RT}{F} ln\left[\frac{P_{NS}[K^+]_i + P_{NS}[Na^+]_i + P_I[I^-]_o + P_{Cl}[Cl^-]_o}{P_{NS}[K^+]_o + P_{NS}[Na^+]_o + P_{Cl}[Cl^-]_i}\right]$$

where P_I is the membrane permeability to I^-, yielded a P_I/P_{Cl} ratio for the adipocyte membrane of 1.6 ± 0.12 ($n = 10$), a value almost identical to that of 1.5 previously described for *V*RAC (32). Moreover, our value of ~0.13–0.14 for the P_{Gluc}/P_{Cl} ratio *Delta* is also similar to that of 0.17 also previously described for *V*RAC (32). Together, these data provide strong evidence in support of a *V*RAC/*V*SOR identity for the predominantly active ion channel in white fat adipocytes. That the different extracellular solutions used in our experiments were almost isosmotic mitigates against the idea that the Cl^- permeability we observed was activated by our experimental conditions.

Lithium permeability of the nonselective cation channel. To control for any nonspecific effects of $NMDG^+$ on *V*m, and to further characterize P_{NS}, we tested the effect of replacement of bath Na^+ with Li^+ on the *V*m of primary adipocytes. Substitution of 138 mM bath Na^+ with Li^+ (292 ± 0.6 mOsm) produced a stable and significant 8.5 ± 1.3 mV ($n = 9$) hyperpolarization ($P < 0.001$, paired *t*-test) of *V*m (Fig. 6*F*). These data suggest that the P_{NS} of primary adipocytes has a lower ionic permeability to Li^+ than to Na^+. Fitting the following form of the GHK equation to our data:

$$Vm = -\frac{RT}{F} ln\left[\frac{P_{NS}[K^+]_i + P_{NS}[Na^+]_i + P_{Cl}[Cl^-]_o}{P_{NS}[K^+]_o + P_{NS}[Na^+]_o + P_{Li}[Li^+]_o + P_{Cl}[Cl^-]_i}\right]$$

where P_{Li} is the membrane permeability to Li^+, gave a P_{Li}/P_{Na} ratio for P_{NS} of 0.49 ± 0.08 ($n = 7$), a value almost identical to that of 0.5 for a nonselective monovalent cation channel described in placental apical membrane (30), for which the P_K/P_{Na} ratio was also 1, a property we observed earlier for the plasma membrane of adipocytes.

Effect of $[Cl^-]_o$ on $[Ca^{2+}]_i$. Depolarization of the plasma membrane by elevation of $[K^+]_o$ is a well-established paradigm used with excitable tissues to increase cytosolic calcium via activation of voltage-gated calcium channels (*V*GCCs). This same methodology has also been extensively applied to white fat adipocytes under the premise that they, too, have a *V*m predominantly controlled by potassium, possessing *V*GCCs, with a resultant increase in $[Ca^{2+}]_i$ with membrane depolarization (15, 18, 27, 36). However, we have previously showed that only 21% of cells give an increase in $[Ca^{2+}]_i$ under similar conditions (38), evidence that suggests the majority of adipocytes either do not possess *V*GCCs or/and have a *V*m that is not controlled by K^+; in this study, we have clearly demonstrated the latter. In primary adipocytes, median basal $[Ca^{2+}]_i$ was 131 nM (103 to 164 nm, 96% CI, $n = 54$; Fig. 9*A*). Figure 9 shows that elevation of $[K^+]_o$, from 5.6 to 50 mM by equimolar substitution of bath Na^+, produced a 29 nM (10 to 45 nm, 96% CI, $n = 40$) increase in $[Ca^{2+}]_i$ ($P < 0.0001$, Wilcoxon test), whereas a decrease in $[Cl^-]_o$ from 152 to 18 mM produced only a 16 nM (10 to 24 nM, 96% CI, $n = 40$) increase in $[Ca^{2+}]_i$ ($P < 0.005$, Wilcoxon test), an effect significantly smaller than that observed with the elevated $[K^+]_o$ ($P < 0.02$, Mann-Whitney; Fig. 9, *B* and *C*). Moreover, when the two experimental paradigms were conducted back to back on the same cell, a larger increase in $[Ca^{2+}]_i$ was still brought about by the elevation of $[K^+]_o$ compared with the decrease in $[Cl^-]_o$: 30 nM (7 to 62 nM, 98% CI, $n = 27$, $P < 0.0001$, Wilcoxon signed rank; Fig. 9*D*). That an elevation of $[K^+]_o$ does not depolarize *V*m suggests that the increase in $[Ca^{2+}]_i$ observed most likely results from reverse Na-Ca exchange (NCX), driven by the low $[Na^+]_i$ concomitant with the elevation of $[K^+]_o$ and not by activation of *V*GCCs. To test this idea, $[Na^+]_o$ was decreased from 138 to 93.6 mM, independently of bath K^+, by equimolar substitution with 44.4 mM $NMDG^+$.

Figure 9*E* illustrates that a decrease in bath Na^+ independent of $[K^+]_o$ increased adipocyte $[Ca^{2+}]_i$, comparable in magnitude to that produced during elevation of bath K^+ to 50 mM (Fig. 9*F*). Moreover, in neither case did 20 μM nifedipine, a specific dihydropyridine inhibitor of *V*GCC, or 10 μM KB-R7943, an inhibitor of reverse NCX, prevent the increase in $[Ca^{2+}]_i$ brought about by a reduction of bath Na^+ either alone or coupled with an increase in $[K^+]_o$ concentration (Fig. 9,*G*, *H*, *I* and *J*). The identity of the mechanism responsible for the small increase in $[Ca^{2+}]_i$ brought about the reduction of $[Cl^-]_o$, and the depolarization of *V*m remains unknown. The depolarization of the *V*m associated with Cl^- removal was expected to cause reverse NCX and increase $[Ca^{2+}]_i$ similar in magnitude to that seen with the partial removal of extracellular Na^+. However, since the increase in $[Ca^{2+}]_i$ observed was only a fraction of that expected suggests that either counter regulatory mechanisms for $[Ca^{2+}]_i$ homeostasis were affected by the change in extracellular anion. Alternatively, the NCX in white fat adipocytes (38) is a unique isoform with a nonelectrogenic $2Na^+:1Ca^{2+}$ stoichiometry, that is insensitive to voltage, and is also insensitive to KB-R7943.

A simple model of adipocyte V*m.* At steady state, the net flux of ionic charge across the plasma membrane of the adipocyte is zero. For simplicity, both Na^+ and K^+ are

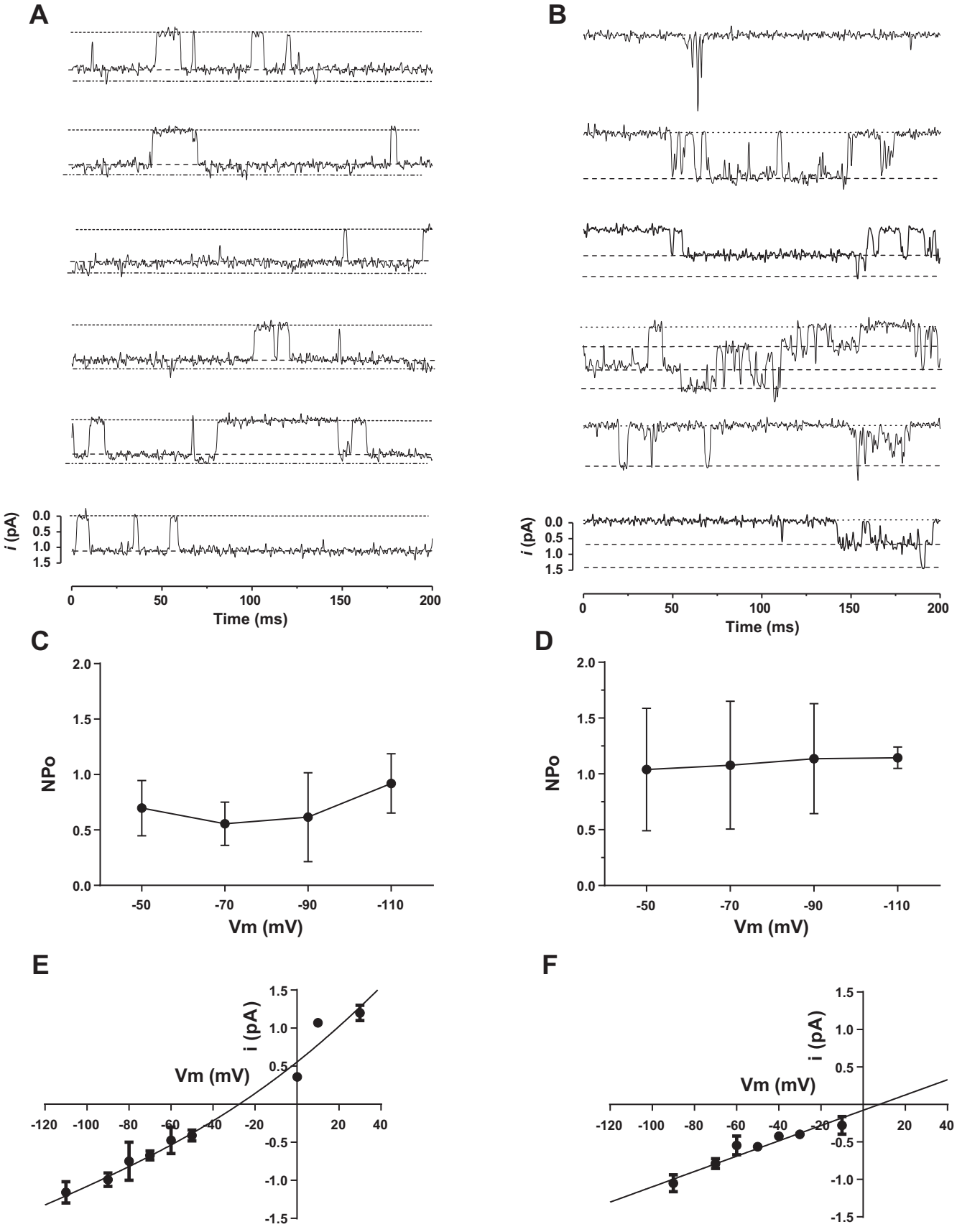
A
B
i (pA)
0.0
0.5
1.0
1.5
0
50
100
150
200
Time (ms)
C
D
NPo
2.0
1.5
1.0
0.5
0.0
-50
-70
-90
-110
Vm (mV)
E
F
i (pA)
Vm (mV)
-120
-100
-80
-60
-40
-20
20
40
-0.5
-1.0
-1.5

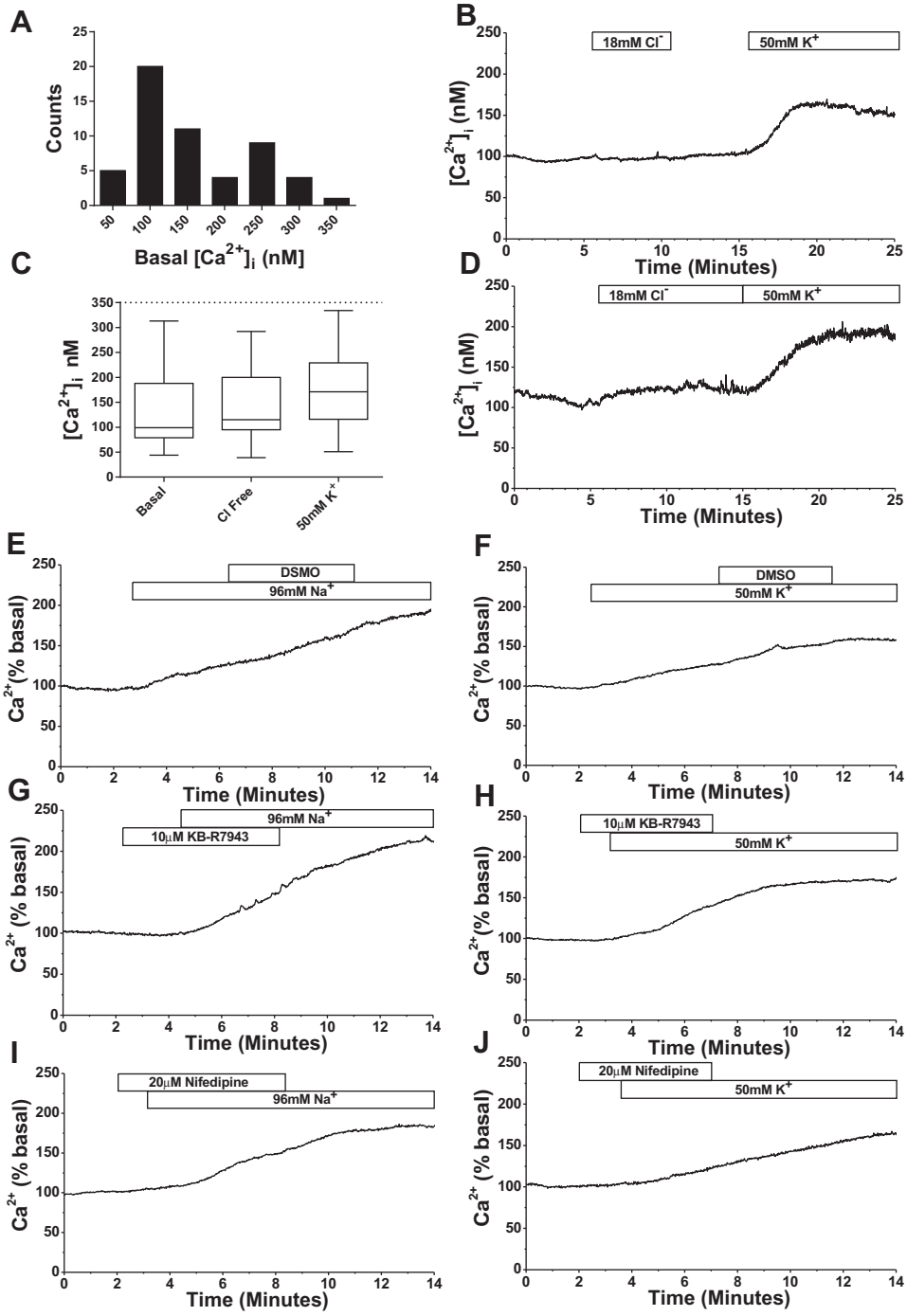

Fig. 9. Effect of ion substitution on $[Ca^{2+}]_i$ of primary adipocytes. *A*: distribution of intracellular calcium concentration, $[Ca^{2+}]_i$ under basal conditions ($n = 54$). *B*: effect of reduction of $[Cl^-]_o$ from 152 to 18 mM followed by a wash and then elevation of $[K^+]_o$ from 5 to 50 mM on the mean $[Ca^{2+}]_i$ from a field of 6 cells. *C*: box and whisker plot comparison for 3 different conditions as indicated on $[Ca^{2+}]_i$ ($n = 27$). *D*: effect of reduction of $[Cl^-]_o$ from 152 to 18 mM directly followed by elevation of $[K^+]_o$ from 5 to 50 mM on the mean $[Ca^{2+}]_i$ from a field of 4 cells. *E*: effect of decreased $[Na^+]_o$, independent of bath K^+ and DMSO on the mean $[Ca^{2+}]_i$ from 4 experiments. *F*: effect of increased $[K^+]_o$ and DMSO on the mean $[Ca^{2+}]_i$ from 6 experiments. *G*: effect of decreased $[Na^+]_o$, independent of bath K^+ in the presence of KB-R7943 on the mean $[Ca^{2+}]_i$, from 8 experiments. *H*: effect of increased $[K^+]_o$, in the presence of KB-R7943 on the mean $[Ca^{2+}]_i$, from 13 experiments. *I*: effect of decreased $[Na^+]_o$, independent of bath K^+ in the presence of nifedipine on the mean $[Ca^{2+}]_i$ from 8 experiments. *J*: effect of increased $[K^+]_o$ in the presence of nifedipine on the mean $[Ca^{2+}]_i$ from 7 experiments.

assumed to permeate via nonselective cation channels. However, since the adipocyte membrane potential is dictated by the passive permeability of both Cl^- and monovalent cations, at the resting *Vm* no ion is at equilibrium; consequently, there will be a net influx of NaCl and an efflux of K^+. For ionic homoeostasis it is envisaged that Na^+ is extruded via the Na^+-K^+-ATPase, whereas excess Cl^- is removed via co-transport with K^+ via KCC, where $[K^+]_i$ is replenished by the Na^+-K^+-ATPase. Since the Na^+-K^+-ATPase is electrogenic, it is necessary to incorporate its

Fig. 8. Single-channel ion activity and related parameters. *A* and *B*: representative recordings of the 2 types of inward single-channel currents' activity measured at a *Vm* of −90 mV; dotted line, closed channel state; dashed line, predominant open-channel state; dot-dashed line, substate. *C* and *D*: open-channel activity, NPo, plotted against holding membrane potential, for the 2 types of channels. Note the lack of voltage dependence in both cases. *E* and *F*: representative single-channel current amplitude-voltage relationship for channel types illustrated above. Solid lines are best fits to the GHK single-channel current equation in E and linear regression in F, with parameters given in text. Data are shown as means ± SE ($n = 8$–11).

contribution to the membrane potential via *r*, the pump ratio in the GHK voltage equation:

$$Vm = -\frac{RT}{F} ln\left[\frac{r[K^+]_{in} + [Na^+]_{in} + \alpha[Cl^-]_{out}}{r[K^+]_{out} + [Na^+]_{out} + \alpha[Cl^-]_{in}}\right]$$

where α is the actual permeability ratio of P_{Cl}/P_{NS} at 4.2, and *r* is the pump ratio of 1.5 for the Na^+-K^+-ATPase (which is taken to have a $3Na^+$:$2K^+$ stoichiometry). Since KCC is electroneutral, it is omitted from the GHK equation.

Conclusion

In conclusion, we have unequivocally demonstrated that the resting membrane potential of isolated identified white fat adipocytes is predominantly controlled by the passive diffusion of Cl^-, most likely via spontaneously active *V*SOR/*V*RAC with a minor contribution from K^+ and Na^+ via nonselective cation channels. Somewhat controversially, our novel data are in contrast to the previous idea that the *V*m of this cell type is predominantly controlled by K^+ (6, 7). Indeed, we now provide a new model from which previous, as well as new data that relate to the membrane physiology of white adipose tissue can be explained. Although insulin did not affect *V*m, isoprenaline depolarized adipocyte *V*m, an observation consistent with an activation of nonselective cation channels. Whether the latter is causal or consequential of β-adrenoceptor-mediated lipolysis is unknown.

The demonstration that manipulation of the transmembrane Cl^- flux causes membrane depolarization has important clinical implications with regard to both the control of the Ca-dependent functions of white fat adipocytes: lipogenesis (29), lipolysis (17, 50), and adipokine secretion such as that of leptin (51). Evidence in support of this idea arises from studies on the use of tamoxifen to treat breast cancer. Tamoxifen is an established inhibitor of *V*RAC (32) and has already been shown to block this channel in human white fat adipocytes (24). Given our demonstration of the key role that anion channels, which we identify to be most probably *V*RAC, play in the membrane physiology of white adipose tissue, we expect that tamoxifen should also lead to a depolarization of white fat adipocytes, elevate their $[Ca^{2+}]_i$, and affect adipokine secretion. Indeed the serum leptin level of patients on tamoxifen is nearly twice that of controls (33), evidence that strongly supports our hypothesis. Since *V*RAC is in fact a multiple target for a plethora of therapeutic drugs (32), metabolic complications that result from aberrant adipocyte function may be explained in part as due to the effects that these drugs have on adipocyte *V*m and $[Ca^{2+}]_i$.

DISCLOSURES

No conflicts of interest, financial or otherwise, are declared by the author(s).

AUTHOR CONTRIBUTIONS

Author contributions: D.C.B., P.P., and P.A.S. performed experiments; D.C.B., P.P., and P.A.S. analyzed data; D.C.B., P.P., and P.A.S. interpreted results of experiments; D.C.B., P.P., S.C., and P.A.S. approved final version of manuscript; S.C. and P.A.S. conception and design of research; S.C. and P.A.S. edited and revised manuscript; P.A.S. prepared figures; P.A.S. drafted manuscript.

REFERENCES

1. **Abercrombie RF, Putnam RW, Roos A.** The intracellular pH of frog skeletal muscle: its regulation in isotonic solutions. *J Physiol* 345: 175–187, 1983.
2. **Adragna NC, Di Fulvio M, Lauf PK.** Regulation of K-Cl cotransport: from function to genes. *J Membr Biol* 201: 109–137, 2004.
3. **Bae YM, Park MK, Lee SH, Ho WK, Earm YE.** Contribution of Ca2+-activated K+ channels and non-selective cation channels to membrane potential of pulmonary arterial smooth muscle cells of the rabbit. *J Physiol* 514: 747–758, 1999.
4. **Bassnett S, Stewart S, Duncan G, Croghan PC.** Efflux of chloride from the rat lens: influence of membrane potential and intracellular acidification. *Exp Physiol* 73: 941–949, 1988.
5. **Beigelman PM, Hollander PB.** Effect of insulin and rat weight upon rat adipose tissue membrane resting electrical potential (REP). *Diabetes* 12: 262–267, 1963.
6. **Beigelman PM, Hollander PB.** Effects of electrolytes upon adipose tissue membrane electrical potentials. In: *Proceedings of the Society for Experimental Biology and Medicine*. New York: Soc Exper Biol Med, vol. 115, no. 1, p. 14–16, 1964.
7. **Beigelman PM, Shu MJ.** Adipose Resting Membrane Potential: In *V*itro Responses to Cl-and K+. In: *Proceedings of the Society for Experimental Biology and Medicine*. New York: Soc Exper Biol Med, vol. 141, no. 2, p. 618–621, 1972.
8. **Betts LC, Kozlowski RZ.** Electrophysiological effects of endothelin-1 and their relationship to contraction in rat renal arterial smooth muscle. *Br J Pharmacol* 130: 787–796, 2000.
9. **Bondarenko A, Sagach V.** Na^+-K^+-ATPase is involved in the sustained Ach-induced hyperpolarization of endothelial cells from rat aorta. *Br J Pharmacol* 149: 958–965, 2006.
10. **Cheng K, Groarke J, Osotimehin B, Haspel HC, Sonenberg M.** Effects of insulin, catecholamines, and cyclic nucleotides on rat adipocyte membrane potential. *J Biol Chem* 256: 649–655, 1981.
11. **Cushman SW.** Structure-function relationships in the adipose cell I. Ultrastructure of the isolated adipose cell. *J Cell Biol* 46: 326–341, 1970.
12. **Daunt M, Dale O, Smith PA.** Somatostatin inhibits oxidative respiration in pancreatic β-cells. *Endocrinology* 147: 1527–1535, 2006.
13. **Dawson CM, Croghan PC, Atwater I, Rojas E.** Estimation of potassium permeability in mouse islets of Langerhans. *Biomed Res* 4: 389–392, 1983.
14. **DiGirolamo M, Owens JL.** Water content of rat adipose tissue and isolated adipocytes in relation to cell size. *Am J Physiol* 231: 1568–1572, 1976.
15. **Draznin B, Kao M, Sussman KE.** Insulin and glyburide increase cytosolic free-Ca2+ concentration in isolated rat adipocytes. *Diabetes* 36: 174–178, 1987.
16. **Duan D, Winter C, Cowley S, Hume JR, Horowitz B.** Molecular identification of a volume-regulated chloride channel. *Nature* 390: 417–421, 1997.
17. **Garcıá-Barrado MJ, Sancho C, Iglesias-Osma MC, Moratinos J.** Effects of verapamil and elgodipine on isoprenaline-induced metabolic responses in rabbits. *Eur J Pharmacol* 415: 105–115, 2001.
18. **Gaur Shikha, Yamaguchi Hiroshi, Goodman HM.** Growth hormone increases calcium uptake in rat fat cells by a mechanism dependent on protein kinase C. *Am J Physiol Cell Physiol* 270: C1485–C1492, 1996.
19. **Gliemann J, Østerlind K, Vinten J, Gammeltoft S.** A procedure for measurement of distribution spaces in isolated fat cells. *Biochim Biophys Acta* 286: 1–9, 1972).
20. **Green H, Kehinde O.** An established preadipose cell line and its differentiation in culture. II. Factors affecting the adipose conversion. *Cell* 5: 19–27, 1975.
21. **Green H, Meuth M.** An established pre-adipose cell line and its differentiation in culture. *Cell* 3: 127–133, 1974.
22. **Goldman DE.** Potential, impedance, and rectification in membranes. *J Gen Physiol* 27: 37–60, 1943.
23. **Hodgkin AL, Horowicz P.** The influence of potassium and chloride ions on the membrane potential of single muscle fibres. *J Physiol* 148: 127, 1959.
24. **Hu H, Li DL, Fan L, Ren J, Wang SP, Jia Zang B, WJ.** Involvement of volume-sensitive Cl^- channels in the proliferation of human subcutaneous pre-adipocytes. *Clin Exper Pharmacol Physiol* 37: 29–34, 2010.

25. **Inoue H, Takahashi N, Okada Y, Konishi M.** *V*olume-sensitive outwardly rectifying chloride channel in white adipocytes from normal and diabetic mice. *Am J Physiol Cell Physiol* 298: C900–C909, 2010.
26. **Jay AWL, Burton AC.** Direct measurement of potential difference across the human red blood cell membrane. *Biophys J* 9: 115–121, 1969.
27. **Kelly KL, Deeney JT, Corkey BE.** Cytosolic free calcium in adipocytes. Distinct mechanisms of regulation and effects on insulin action. *J Biol Chem* 264: 12754–12757, 1989.
28. **Lee SC, Pappone PA.** Membrane responses to extracellular ATP in rat isolated white adipocytes. *Pflügers Arch* 434: 422–428, 1997.
29. **Li Y, Wang P, Xu J, Desir GV.** *V*oltage-gated potassium channel Kv1.3 regulates GLUT4 trafficking to the plasma membrane via a Ca^{2+}-dependent mechanism. *Am J Physiol Cell Physiol* 290: C345–C351, 2006.
30. **Llanos P, Henriquez M, Riquelme G.** A low conductance, non-selective cation channel from human placenta. *Placenta* 23: 184–191, 2002.
31. **McCarty NA, Zhang ZR.** Identification of a region of strong discrimination in the pore of CFTR. *Am J Physiol Lung Cell Mol Physiol* 281: L852–L867, 2001.
32. **Nilius B, Droogmans G.** Amazing chloride channels: an overview. *Acta Physiol Scand* 177: 119–147, 2003.
33. **Ozet A, Arpaci F, Yilmaz MI, Ayta H, Ozturk B, Komurcu S, Acikel C.** Effects of tamoxifen on the serum leptin level in patients with breast cancer. *Jpn J Clin Oncol* 31: 424–427, 2001.
34. **Perry MC, Hales CN.** Rates of efflux and intracellular concentrations of potassium, sodium and chloride ions in isolated fat-cells from the rat. *Biochem J* 115: 865, 1969.
35. **Perry MC, Hales CN.** Factors affecting the permeability of isolated fat-cells from the rat to [^{42}K] potassium and [^{36}Cl] chloride ions. *Biochem J* 117: 615, 1970.
36. **Pershadsingh HA, Lee LY, Snowdowne KW.** Evidence for a sodium/calcium exchanger and voltage-dependent calcium channels in adipocytes. *FEBS Lett* 244: 89–92, 1989.
37. **Price EM, Gabriel SE, Stutts MJ, Boucher RC, Larsen EH.** Clusters of Cl^- channels in CFTR-expressing Sf9 cells switch spontaneously between slow and fast gating modes. *Pflügers Arch* 432: 528–537, 1996.
38. **Pulbutr P, Chan SLF, Smith PA.** Evidence of Ca^{2+} entry pathways in rat white adipocytes. *Fundam Clin Pharmacol* 22: 94–94, 2008.
39. **Ramírez-Ponce MP, Acosta J, Bellido JA.** Electrical activity in white adipose tissue of rat. *Revista Española Fisiol* 46: 133, 1990.
40. **Ringer E, Russ U, Siemen D.** β_3-Adrenergic stimulation and insulin inhibition of non-selective cation channels in white adipocytes of the rat. *Biochim Biophys Acta* 1463: 241–253, 2000.
41. **Rodbell M.** Metabolism of isolated fat cells. I. Effects of hormones on glucose metabolism and lipolyis. *J Biol Chem* 239: 375–380, 1964.
42. **Smith PA, Ashcroft FM, Rorsman P.** Simultaneous recordings of glucose dependent electrical activity and ATP-regulated K^+-currents in isolated mouse pancreatic β-cells. *FEBS Lett* 261: 187–190, 1990.
43. **Smith PA, Aschroft FM, Fewtrell CM.** Permeation and gating properties of the L-type calcium channel in mouse pancreatic beta cells. *J Gen Physiol* 101: 767–797, 1993.
44. **Stark RJ, Read PD, O'Doherty J.** Insulin does not act by causing a change in membrane potential or intracellular free sodium and potassium concentration of adipocytes. *Diabetes* 29: 1040–1043, 1980.
45. **Sterratt D, Graham B, Gillies A, Willshaw D.** *Principles of Computational Modelling in Neuroscience*. London: Cambridge Univ. Press, 2011.
46. **Stauber T, Weinert S, Jentsch TJ.** Cell biology and physiology of CLC chloride channels and transporters. *Comprehens Physiol* 2: 1701–1744, 2012.
47. **Thorsteinsson B, Gliemann J, Vinten J.** The content of water and potassium in fat cells. *Biochim Biophys Acta Gen Subj* 428: 223–227, 1976.
48. **Weinreich F, Jentsch TJ.** Pores formed by single subunits in mixed dimers of different CLC chloride channels. *J Biol Chem* 276: 2347–2353, 2001).
49. **Williamson JR.** Adipose tissue morphological changes associated with lipid mobilization. *J Cell Biol* 20: 57–74, 1964.
50. **Xue B, Greenberg AG, Kraemer FB, Zemel MB.** Mechanism of intracellular calcium ([Ca2+]i) inhibition of lipolysis in human adipocytes. *FASEB J* 15: 2527–2529, 2001.
51. **Ye F, Than A, Zhao Y, Goh KH, Chen P.** *V*esicular storage, vesicle trafficking, and secretion of leptin and resistin: the similarities, differences, and interplays. *J Endocrinol* 206: 27–36, 2010.